Isotropic nanocrystalline $Sm(Fe,Co)_{11.3}Ti_{0.7}$ magnets modified with B and Zr

A.M. Gabay*, G.C. Hadjipanayis
Department of Physics and Astronomy, University of Delaware, Newark, Delaware 19716, USA

Rare-earth-lean $Sm(Fe,Co,Ti)_{12}$ alloys with the $ThMn_{12}$ crystal structure and less than one Ti atom per formula unit have the potential of exceptionally powerful permanent magnets, but all prior attempts to develop high coercivity in bulk alloys, especially coercivity combined with crystallographic texture, have fallen short of the expectations. This study was aimed at improvement of the currently best $Sm(Fe,Co,Ti)_{12}$ magnets prepared through melt-spinning which are inherently isotropic. Modifications of the alloys with B and Zr, already demonstrated in earlier studies to be effective separately, have been implemented simultaneously. A systematic study of $Sm_{1.1-x}(Fe,Co)_{11.3-y}Ti_{0.7}B_y$ alloys melt-spun at a tangential speed of 50 m/s and annealed at 600–950 °C allowed for monitoring the continuous evolution of the two consecutive crystal structures, those of the $TbCu_7$ and $ThMn_{12}$ types. Zirconium was found to facilitate the formation of the 1:12 structure at the expense of the 1:7, whereas boron has the opposite effect, at certain concentrations completely suppressing the 1:12. When the two alloying elements are introduced simultaneously, they inhibit growth of the 1:12 crystallites at annealing temperatures higher than 800 °C, thus allowing for the development of a higher coercivity. Because of instrumental limitations, bulk magnets were prepared through a two-step process – compaction of the melt-spun ribbons at 650 °C and additional treatment at a higher temperature – and they were characterized by a reduced, 90–93%, density. Nevertheless, an isotropic $Sm_{0.9}Zr_{0.2}(Fe,Co)_{10.8}Ti_{0.7}B_{0.5}$ magnet exhibited fair values of the remanence (7.4 kG), maximum energy product (8.5 MGOe) and coercivity (5.4 kOe), as well as high Curie temperature of 525 °C and remarkably small temperature coefficient of the coercivity, -0.25%/°C.

Keywords: permanent magnets; $ThMn_{12}$ structure; nanostructured materials; melt-spinning; hot compaction.

*Corresponding author at: University of Delaware, 217 Sharp Lab, Newark, DE 19716, USA.
E-mail address: gabay@udel.edu (A.M. Gabay).

1. Introduction

Several recently synthesized tetragonal compounds isostructural to the $ThMn_{12}$ and based on $Sm(Fe,Co)_{12}$ [1–5] offer intrinsic magnetic properties at a level which is very attractive for the development of rare-earth-lean, high-temperature permanent magnets. In the absence of epitaxy [2], iron-rich 1:12 compounds are stabilized by the addition of certain non-magnetic elements which occupy part of the 3d-transition-metal sites; among these stabilizing elements, Ti stands out for allowing the highest saturation magnetization M_s. The M_s of the $Sm(Fe,Co,Ti)_{12}$ compounds becomes particularly advantageous for Ti concentrations smaller than 1 atom per formula unit [1,3,4,6], and it is worth reminding that the minimum Ti concentration in the $Sm(Fe,Ti)_{12}$ compounds was determined to be 0.7 atom per formula unit at 1000 °C [7]. Several other modifications have been experimentally and theoretically demonstrated to lower the formation energy of the 1:12 structure, particularly, the Zr atoms occupying part of the rare-earth sites [8,9]. Despite the strong magnetocrystalline anisotropy characteristic of the $Sm(Fe,Ti)_{12}$ and derivative alloys, development of practically useful coercivity H_c in these materials proved to be difficult. This underperformance still lacks universally accepted explanation; different studies attributed it to unfavorable phase equilibria [7,10], propensity to twinning [11] and magnetism of the grain boundaries [12]. The initial efforts to develop useful coercivity in the $Sm(Fe,Ti)_{12}$ and $Sm(Fe,Co,Ti)_{12}$ alloys through melt-spinning followed by annealing at 800–850 °C generated H_c values of 5–6 kOe [6,13–17]. Recent attempts to apply the same technique to "Ti-lean" and/or Zr-substituted alloys resulted in lower H_c values of 3–5 kOe [18–22], although a subsequent interstitial modification of the $Sm_{1.2-x}Zr_xFe_{10}Ti$ ribbons with hydrogen was reported to increase their H_c to 7 kOe [20].

Somewhat higher H_c values were realized in the 1990s in melt-spun and annealed $Sm(Fe,Ti)_{12}$ alloys modified with boron: 7.7 kOe in $Sm_{1.3}Fe_{10.7}TiB_{0.3}$ [23] and 6.0 kOe in $SmFe_{10.8}Ti_{1.2}B_{0.2}$ [24]. The mechanism of the boron influence was not investigated in those studies beyond the observation of increased glass-forming ability. The currently available experimental data for boron-modified 1:12 structures are limited to a $Y(Fe,Ti,B)_{12}$ compound [25] and $RFe_{10}V_2B_{0.5}$ compounds with R represented by Y, Nd and Sm [26]; in both reports the B atoms were claimed to occupy the 3d-transition-metal sites. According to recent density-functional theory calculations [27], *interstitial* B atoms should lower the formation energy of the $SmFe_{12}$ compound, although not enough for the compound to become thermodynamically stable. Indeed, no 1:12 structures were detected in melt-spun $Sm_{0.7}Zr_{0.3}(Fe_{0.8}Co_{0.2})_{11}B_{0–1.0}$ [28] and $SmFe_{12}B_{0–1.5}$ [29] alloys, where the added boron increased the glass-forming ability and somewhat improved the moderate hard-magnetic properties associated with a hexagonal structure of the $TbCu_7$-type [30]. On the other hand, addition of boron remarkably increased H_c – from 1 kOe to 12 kOe – of epitaxially grown $Sm(Fe_{0.8}Co_{0.2})_{12}$ thin film, supposedly by insulating the 1:12 nanograins with a B-rich amorphous phase [31].

Although coercivity enables operation of the permanent magnet, the energy stored by this magnet is primarily determined by its remanence B_r. The most natural way to ensure high B_r

values is to align the easy-magnetization directions of the crystallites. Several reported attempts to prepare *anisotropic* $Sm(Fe,[Co,]M)_{12}$ magnets with M = Ti, V, Mo through sintering of oriented powders or through hot plastic deformation of nanocrystalline alloys produced results which fell short of the expectations: the coercivity obtained in the sintering experiments was only 2.0–3.2 kOe [32,33], whereas the degree of the [001] texture developed via the hot deformation was too low to make a difference [34–36]. Manufacturing of *isotropic* 1:12 magnets has been explored as well – by compacting high-energy milled [34] or melt-spun [37–39] nanocrystalline alloys; in some cases, an additional post-compaction annealing was necessary to complete the formation of the 1:12 structure [34,39]. The most interesting data were reported recently for a $Sm(Fe_{0.8}Co_{0.2})_{11}Ti$ melt-spun alloy compacted at room temperature with a high pressure of 12.5 GPa and subsequently annealed at 800 °C [39]: relatively large B_r values of 9.0–9.4 kG and maximum energy product $(BH)_{max}$ ≈10 MGOe, with a 12.2 MGOe value measured in one outlying sample. The largest H_c realized in that experiment, 3.9 kOe, was consistent with the other reports for the nanocrystalline $Sm(Fe,Co,Ti)_{12}$ alloys, but it was rather low for practical applications.

In this work, the effects of Zr and B substitutions on the structure and magnetic properties are investigated for melt-spun and annealed alloys based a "Ti-lean" $Sm_{1.1}(Fe_{0.8}Co_{0.2})_{11.3}Ti_{0.7}$ composition. Structural changes in the $TbCu_7$- and $ThMn_{12}$-type structure occurring in the course of the annealing are systematically monitored. The results obtained for annealed melt-spun ribbons are then used to optimize the preparation of bulk isotropic magnets.

2. Experiment

Alloys of the nominal compositions $(Sm_{1-x}Zr_x)_{1.1}(Fe_{0.8}Co_{0.2})_{11.3-y}Ti_{0.7}B_y$ with x = 0, 0.2 and y = 0, 0.3, 0.5, 0.7 were prepared by arc-melting under argon atmosphere from Sm (99.9%), Zr (99.2%), Fe (99.97%), Co (99.9%), Ti (99.5%) and B (99.5%). To reduce evaporation loss of Sm (the loss was compensated by adding 15 wt.% excess of Sm over the nominal amount), Zr and B were introduced not directly, but through pre-fabricated $Fe_{90}Zr_{10}$ and $Fe_{83}B_{17}$ eutectic alloys. The alloys were re-melted 3 to 6 times to ensure both a macroscopic chemical homogeneity and the matching of the actual and intended masses. Melt-spinning was done under argon by ejecting inductively melted alloys through a 0.3–0.4 mm orifice onto a rotating Cu wheel with a wheel tangential velocity of 50 m/s. For heat-treatment, the melt-spun "ribbons" sealed in quartz capsules under vacuum (typically for annealing temperatures T_a < 800 °C) or in argon (T_a ≥ 800 °C), then placed into furnace preheated to the T_a for 15 min or other specified period of time and finally quenched in water. For hot compaction, mortar-ground ribbons were placed into a resistively heated tungsten-carbide die and heated in vacuum to 650 °C under a 300 MPa unidirectional pressure. The temperature and the pressure were maintained for 15 min. The compacted ribbons were annealed similarly to the loose ones but typically for a longer time of 60 min.

Phase compositions and crystal-structure data were determined from X-ray diffraction (XRD) patterns; the latter were recorded for mortar-ground powder specimens with a Rigaku Ultima IV diffractometer using the Cu Kα radiation and analyzed with Powder Cell software [40]. Magnetic phases were additionally characterized via thermogravimetric analysis in a magnetic field with a modified PerkinElmer Diamond instrument. Mean crystallite sizes were estimated through the Scherrer equation [41]; a Gaussian correction was applied to the broadening of the measured XRD peaks to remove the instrumental broadening determined with a Si standard. Crystallites were also observed on fractured surfaces of alloy samples with scanning electron microscopy (SEM) using a JEOL JSM-6335F instrument. Demagnetization curves were measured between 27 °C (hereinafter, "room temperature") and 425 °C with a Quantum Design VersaLab vibrating sample magnetometer after magnetizing the specimens with a pulsed field of 100 kOe. Ribbon specimens (typically 3–5 stacked ribbon pieces measured "in-plane") were assumed to have zero demagnetization factor. Bulk specimens were cut as rectangular prisms, and their demagnetization curves were corrected with the magnetometric demagnetization factors [42]. Densities were measured with the Archimedes method.

3. Results and discussion

3.1. Phase composition of melt-spun and annealed ribbons

Four crystal structures were identified in the XRD pattern of the arc-melted parent $Sm_{1.1}(Fe_{0.8}Co_{0.2})_{11.3}Ti_{0.7}$ alloy. The pattern is shown in Fig. 1(a), and the phase composition data obtained through Rietveld refinement are specified in Table S1, Supplementary data. The 1:12 structure (space group I4/mmm) makes the majority phase accounting for some 83% of the alloy volume, with 16 vol.% of the 1:7 phase (P6/mmm) and a trace amount of the $SmFe_2$ cubic Laves phase (Fd-3m) detected as well. The 1:7 structure can be seen as a *solid solution* of "dumbbell" pairs of 3d-transition-metal atoms in the structure of the $CaCu_5$ type, where the "dumbbells" replace randomly a fraction *r* of the rare-earth atoms. The "1:7" notation used in this work is a reference to the $TbCu_7$ prototype structure synthesized with $r = 0.22$ [43]; the actual *r* value of the specific 1:7 phase must depend on the composition of the alloy. Other notations like "1:9" [30] and "$CaCu_5$-type phase " [44] were used for the same solid solution compound in earlier reports. The 1:7 structure with $r = 0.5$ is identical to *disordered* 1:12 structure [45], which means that the two structures can be transformed into each other by ordering or disordering the "dumbbells." Indeed, both 1:12 → 1:7 and 1:7 → 1:12 transitions were observed in melt-spun $Sm(Fe,Ti)_{12}$ alloys with increasing solidification rate [46] and with annealing of the of the solidified alloys [17], respectively. That the fundamental reflections of the 1:12 and 1:7 XRD patterns often match increases the uncertainty of the XRD analysis. In order to verify the XRD refinement data, the as-prepared $Sm_{1.1}(Fe_{0.8}Co_{0.2})_{11.3}Ti_{0.7}$ alloy was also subjected to the thermomagnetic characterization, which is shown in Fig. 2(a). The two observed Curie temperatures, T_{C1} of 457 °C and T_{C2} of 524 °C, apparently correspond to the 1:7 and 1:12 phases,

respectively; this observation is consistent with the earlier reports that in the $Sm(Fe,Ti)_{12}$ [17,46] and $Sm(Fe,Co,Ti)_{12}$ [44] alloys, the $T_C^{1:7}$ is 30–80 °C lower than the $T_C^{1:12}$.

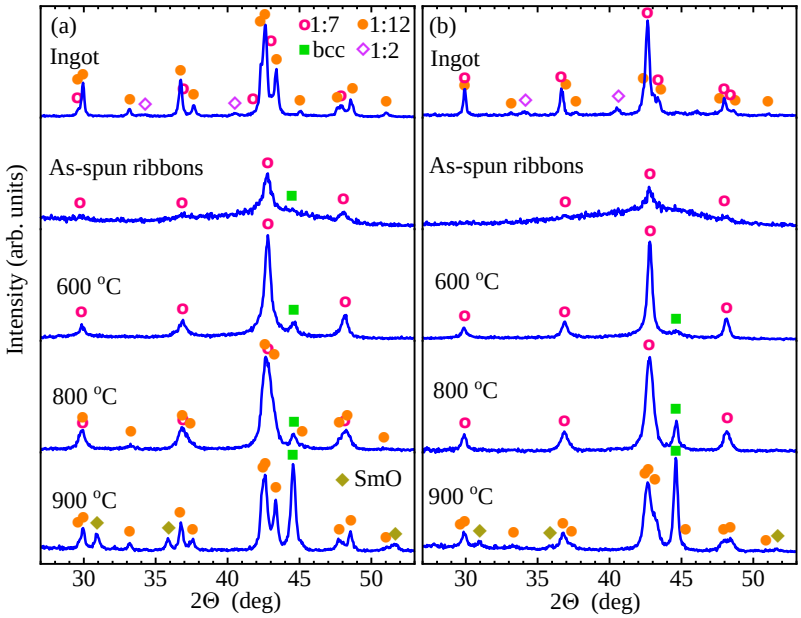

Fig. 1. Selected powder XRD patterns of $Sm_{1.1}(Fe_{0.8}Co_{0.2})_{11.3-y}Ti_{0.7}B_y$ alloys for (a) $y = 0$ and (b) $y = 0.3$: as-prepared, melt-spun and annealed after the melt-spinning at the indicated temperature. The identified crystal structures belong to the $TbCu_7$ ("1:7"), $ThMn_{12}$ ("1:12"), $MgCu_2$ ("1:2"), W ("bcc"), and NaCl ("SmO") types.

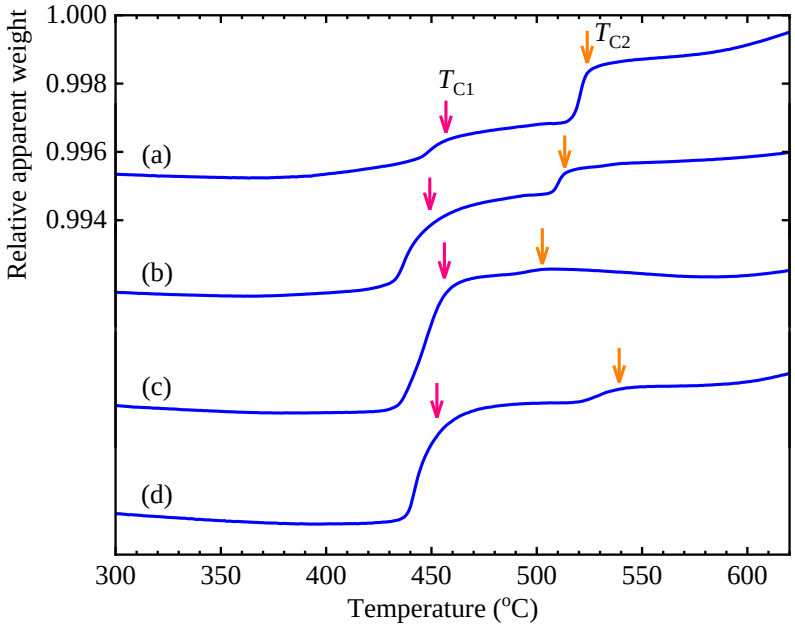

Fig. 2. Heating thermogravimetric curves recorded in a magnetic field for as-prepared $Sm_{1.1-x}Zr_x(Fe_{0.8}Co_{0.2})_{11.3-y}Ti_{0.7}B_y$ ingots with (a) $x = 0$, $y = 0$; (b) $x = 0$, $y = 0.3$; (c) $x = 0$, $y = 0.7$; (d) $x = 0.2$, $y = 0.7$. Curves (b)-(d) are displaced for clarity.

Ribbons produced through the melt-spinning were 10–12 μm thick. In the parent $Sm_{1.1}(Fe_{0.8}Co_{0.2})_{11.3}Ti_{0.7}$ alloy, the melt-spinning suppressed the formation of the ordered 1:12 structure and generated an amorphous phase – coexisting, however, with the 1:7 phase and a trace amount of bcc structure (Im-3m, an Fe-rich Fe-Co phase). Evolution of the phases in the annealed ribbons with the annealing temperature is consistent with earlier studies [17,44,46]: the 1:7 phase dominates in the ribbons annealed at 600–750 °C, whereas the 1:12 phase is first detected for T_a = 800 °C. As the T_a increases, the bcc phase becomes more prominent, apparently because of evaporation and oxidation of Sm at the ribbon surfaces. That oxidation is taking place is evidenced by a SmO oxide phase (Fm-3m) detected for $T_a \geq 850$ °C.

Introduction of boron into $Sm_{1.1}(Fe_{0.8}Co_{0.2})_{11.3-y}Ti_{0.7}B_y$ *ingots* shifts the ratio between the 1:12 and 1:7 phases towards the latter. For y = 0.3, the 1:7 phases accounts for 72% of the alloy volume and for y = 0.7 it accounts for 93%; the corresponding XRD patterns are shown in Fig. 1(b) and Fig 3(a). This shift towards the 1:7 phase can also be seen in the thermomagnetic data, Fig. 2(a)-(c). That the Curie temperature of the 1:12 phase, T_{C2}, decreases with y seems to disagree with report by Chuang et al. [26] that boron *increases* Curie temperature of the $Sm(Fe,V,B)_{12}$ compounds. However, the composition of the 1:12 phase is not necessarily proportional to composition of the alloy, especially when the 1:12 is no longer the majority phase. In the melt-spun ribbons, boron expectedly promotes the amorphous phase, which becomes the only phase detected in the ribbons with y = 0.7. The formation of the 1:12 phase in *annealed* ribbons is delayed in the ribbons with y = 0.3, where it begins only at T_a = 850 °C, and it is completely suppressed in the ribbons with y = 0.7. Even though the neutron diffraction data reported by Zhang et al. [25] for the $Y(Fe,Ti,B)_{12}$ alloy place the boron atoms in the 8i sites of the 1:12 structure, and Zheng et al. [29] found boron stabilizing the 1:7 structure even in Ti-free melt-spun $SmFe_{12}B_y$ alloys, the presented data can not completely rule out the possibility that part of the added boron binds the Ti atoms into a (undetected) TiB_2 phase; the latter would also suppress the 1:12 phase – by depleting it of Ti.

The effect of zirconium on the relative stabilities of the 1:7 and 1:12 phases is opposite to that of boron. Annealing at a lower T_a of 800 °C is sufficient to completely replace the 1:7 structure with the 1:12 structure in the $Sm_{0.9}Zr_{0.2}(Fe_{0.8}Co_{0.2})_{11.3}Ti_{0.7}$ ribbons (as compared to 850 °C for ribbons of the parent composition). In the boron-containing alloys, Zr restores the 1:12 structure suppressed by boron, as it is evident from comparison of the XRD patterns presented in Fig 3(b) and Fig. 3(a), as well as from comparison of thermomagnetic data (d) and (c) in Fig. 2. Note that the Curie temperature of the "restored" 1:12 phase, T_{C2}, is increased to 539 °C. This tendency of the partial Zr substitution for Sm to stabilize the $ThMn_{12}$-type structure is similar to the findings by Kobayashi et al. [8] and Tozman et al. [3] for the $Sm_{1-x}Zr_x(Fe,Co,Ti)_{12}$ alloys; it is also consistent with ab initio calculations of formation energy for hypothetical $Sm_{1-x}Zr_xFe_{12}$ compounds reported by Harashima et al. [9].

Recently, Suzuki [47] was able to present the evolution of the hexagonal 1:7 structure in quasi-binary $Y(Fe,Co)_z$ alloys towards the tetragonal 1:12 structure as a continuous distortion of

a lower-symmetry orthorhombic structure. While being a powerful research tool, this model would overly complicate consideration of the multicomponent alloys studied in the present work. The authors, therefore, have opted for a more conservative approach considering separately the changes of the *a* and *c* lattice parameters of the 1:7 and 1:12 structures, but then merging the results under the assumption that the 1:7 → 1:12 transformation converts $a_{1:7}$ into $c_{1:12}$ and $2c_{1:7}$ into $a_{1:12}$ [45,46]. The corresponding graphs shown in Fig. 4 demonstrate a continuous increase of the $2c_{1:7}$ and $a_{1:12}$ with a relatively smooth transition of the former into the latter. In contrast, the $a_{1:7}$ experiences little change and its transition into the c_{12} is rather drastic. The $Sm_{1.1}(Fe,Co)_{10.6}Ti_{0.7}B_{0.7}$ alloy, in which the 1:12 structure could not be formed, clearly breaks this pattern.

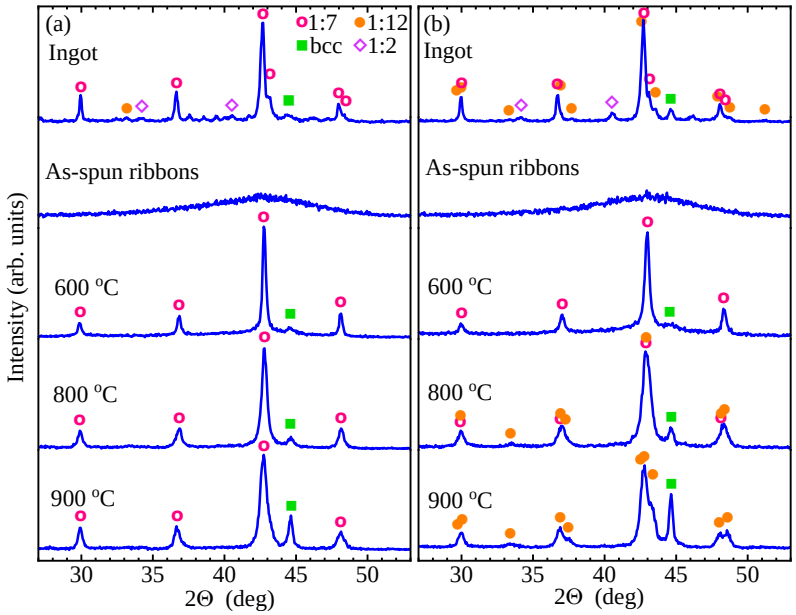

Fig. 3. Selected powder XRD patterns of $Sm_{1.1-x}Zr_x(Fe_{0.8}Co_{0.2})_{10.6}Ti_{0.7}B_{0.7}$ alloys for (a) $x = 0$ and (b) $x = 0.2$: as-prepared, melt-spun and annealed after the melt-spinning at the indicated temperature. The identified crystal structures belong to the $TbCu_7$ ("1:7"), $ThMn_{12}$ ("1:12"), $MgCu_2$ ("1:2"), and W ("bcc").

Further insights into the 1:7 → 1:12 transformation and the effects of alloying with B and Zr can be gained from consideration of a $c_{1:12}/a_{1:12}$ unit cell aspect ratio and its "precursor" $a_{1:7}/2c_{1:7}$, plotted together in Fig. 5. For the melt-spun $Sm_{1.1}(Fe,Co)_{11.3}Ti_{0.7}$ ribbons this "generalized" aspect ratio gradually decreases with the T_a from approximately $1/\sqrt{3}$, which is known to be the critical value signifying the reversed 1:12 → 1:7 transformation [46], to the values observed in arc-melted ingots. Introduction of boron first shifts the aspect ratio towards the $1/\sqrt{3}$ threshold ($y = 0.3$) effectively delaying the formation of the 1:12 structure and then raises it above $1/\sqrt{3}$ ($y = 0.7$) thus preventing the formation of the 1:12 structure altogether.

Conversely, introduction of zirconium tends to shift the aspect ratio away from the $1/\sqrt{3}$ threshold, in effect facilitating the formation of the 1:12 structure.

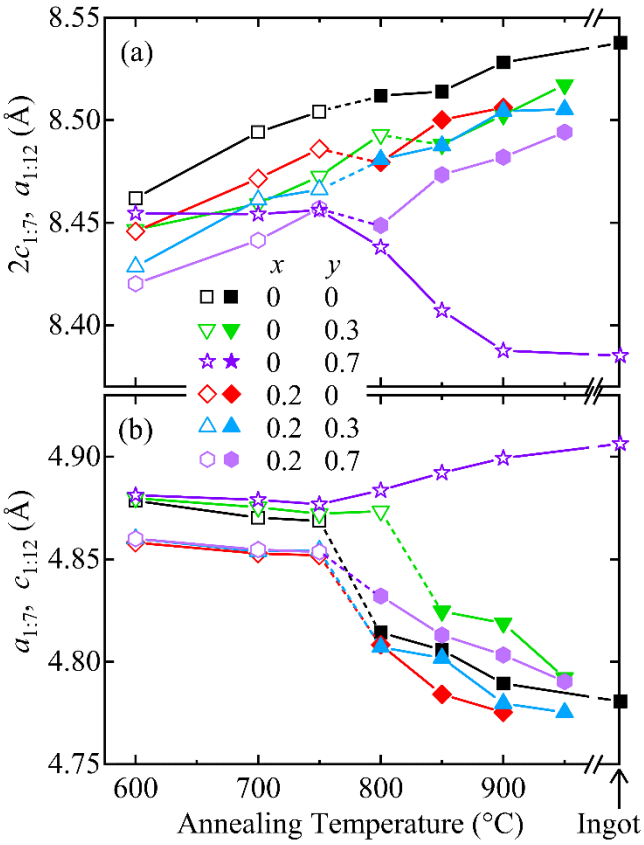

Fig. 4. Evolution of lattice parameters of 1:7 structure (open symbols) and 1:12 structure (filled symbols) in $Sm_{1.1-x}Zr_x(Fe_{0.8}Co_{0.2})_{11.3-y}Ti_{0.7}B_y$ ribbons with annealing temperature (annealing for 15 min).

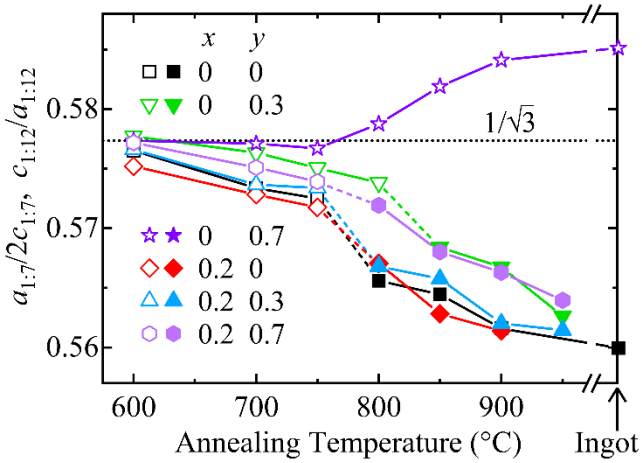

Fig. 5. Evolution of lattice parameter ratios $a_{1:7}/2c_{1:7}$ (open symbols) and $c_{1:12}/a_{1:12}$ (filled symbols) in $Sm_{1.1-x}Zr_x(Fe_{0.8}Co_{0.2})_{11.3-y}Ti_{0.7}B_y$ ribbons with annealing temperature (annealing for 15 min).

3.2. Magnetic properties of melt-spun and annealed ribbons

The as-spun ribbons and those annealed at 500 °C were found to be magnetically soft with a room-temperature H_c smaller than 100 Oe (smaller than 10 Oe when fully amorphous). The hard magnetic properties are first observed in ribbons annealed at 600 °C, which coincides with the crystallization of the 1:7 phase. Figure 6 presents a selection of the typical demagnetization curves recorded for the parent alloy and one of the compositionally modified alloys after annealing at 600–950 °C. Figure 7 summarizes the H_c data for all eight studied $Sm_{1.1-x}Zr_x(Fe,Co)_{11.3-y}Ti_{0.7}B_y$ alloys. The emerging H_c increases with the T_a, somewhat lagging behind in the case of the ribbons solidified with a residual crystalline phase (such as for the ribbons of the parent composition). The 1:7 phase crystallized during annealing is thus associated with a larger H_c than the 1:7 phase crystallized during melt-spinning. However, this difference in H_c almost disappears in the ribbons annealed at 750 °C, the last T_a before the onset of the 1:12 phase. In the alloys experiencing the 1:7 → 1:12 transformation, the increase of H_c with the T_a continues, whereas in the $Sm_{1.1}(Fe,Co)_{10.6}Ti_{0.7}B_{0.7}$ alloy, in which this transformation is suppressed, the H_c levels off at 2.5–2.7 kOe. As one can see in Fig. 7(a), boron does not improve the magnetic hardness of the *zirconium-free* alloys which reach their maximum H_c after annealing at 800–850 °C, and this H_c does not exceed 4.8 kOe. On the other hand, introduction of boron *simultaneously with zirconium* [Fig. 7(b)] increases both the optimum T_a to 900 °C and the maximum H_c to 6.2 kOe. Most ribbon samples annealed at T_a > 800 °C exhibited a zero-field step on their demagnetization curves (see Fig. 6); these steps are believed to reflect the increasing volume fraction of the magnetically soft bcc phase due to evaporation and/or oxidation of Sm. Although annealing at high T_a leads also to a sharp decline of the H_c (see Fig. 7), it is clear from Fig. 6 that the zero-field magnetization steps (i.e., the bcc phase) are *not* the major reason for this decline. It may also be noted that the B_r peaks at lower T_a values than the H_c does, and that in most cases this "early" decline of the B_r cannot be attributed to the zero-field magnetization step.

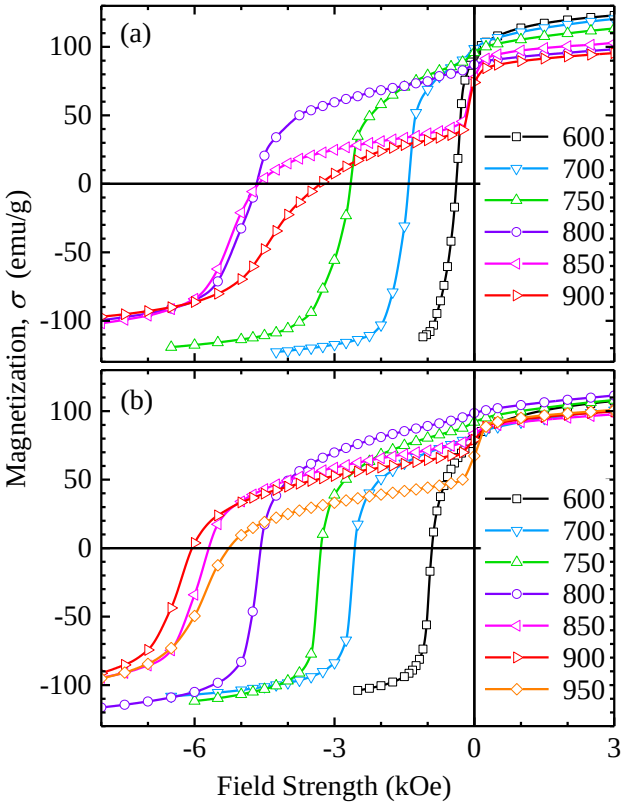

Fig. 6. Room-temperature demagnetization curves of (a) $Sm_{1.1}(Fe_{0.8}Co_{0.2})_{11.3}Ti_{0.7}$ and (b) $Sm_{0.9}Zr_{0.2}(Fe_{0.8}Co_{0.2})_{10.6}Ti_{0.7}B_{0.7}$ melt-spun ribbons annealed for 15 min at the indicated temperatures (in °C).

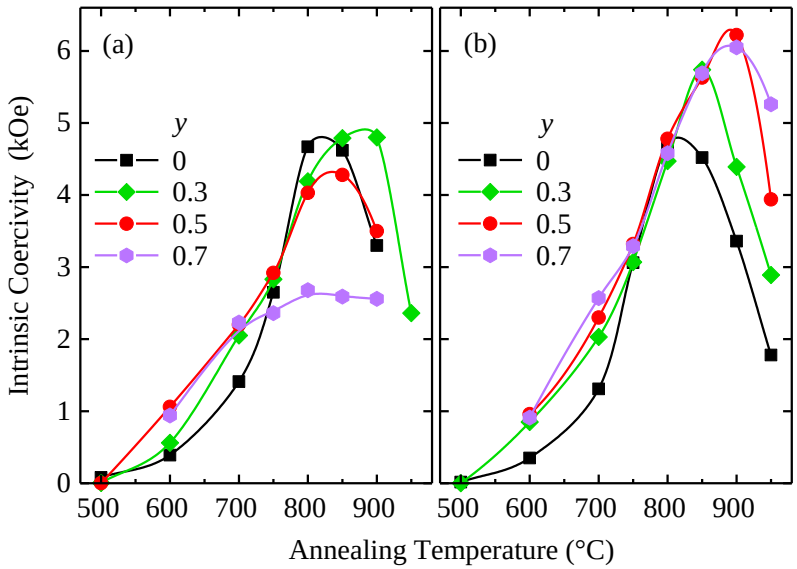

Fig. 7. Effect of 15-min annealing on intrinsic coercivity of (a) $Sm_{1.1}(Fe_{0.8}Co_{0.2})_{11.3-y}Ti_{0.7}B_y$ and (b) $Sm_{0.9}Zr_{0.2}(Fe_{0.8}Co_{0.2})_{11.3-y}Ti_{0.7}B_y$ melt-spun ribbons.

In general, coercivity is determined by both properties of the involved compounds and the morphology of their crystallites (the microstructure). Only limited data are currently available on how Zr substitution affects the intrinsic properties of the $Sm(Fe,Co,Ti)_{12}$ compounds [1,3,48] and no data at all on the effects of B or (B,Zr). All melt-spun alloys which developed the 1:12 structure in this study exhibited similar H_c values after annealing at 800 °C (Fig. 7). With the lattice parameters of the 1:12 structures evolving in the same direction (Fig. 4), the significant H_c difference for the T_a > 800 °C most probably arise not from changing intrinsic properties, but from the continuing development of the microstructure. Figure 8 compares the average crystallite sizes and fractions of the bcc phase determined from the XRD data for the ribbons exhibiting significantly different H_c values. Because of considerable overlap of the XRD reflections, the Scherrer analysis had to be applied to the stand-alone but weak (310) reflection; this resulted in large uncertainties of the determined average sizes [the only exception was the sample annealed at 950 °C which had a stronger (301) reflection sufficiently separated to be analyzed]. Despite the uncertainty, it is clear that the (B,Zr) substitution significantly inhibits the growth of the 1:12 crystallites. Matzinger et al. [49] reported inhibition of crystallite growth in Nd–Fe–B–Zr alloys due to the presence of platelet-shaped ZrB_2 precipitates in intergranular regions. The same mechanism could hypothetically operate in the alloys studied in this work, provided that the amount of the ZrB_2 phase is below the XRD detection threshold. Inhibition of crystallite growth explains the higher H_c values of the compositionally modified alloys more consistently than a smaller fraction of the bcc phase. Even though the fraction of this soft magnetic phase *is* smaller in the modified alloy, in none of the two alloys the observed changes of the H_c are correlated with changes of this fraction. Such lack of correlation is possible because as long as the bcc phase is responsible for less than half of the alloy magnetization, it primarily manifests itself as a zero-field step on the demagnetization curve (see Fig. 6) and only marginally affects the H_c.

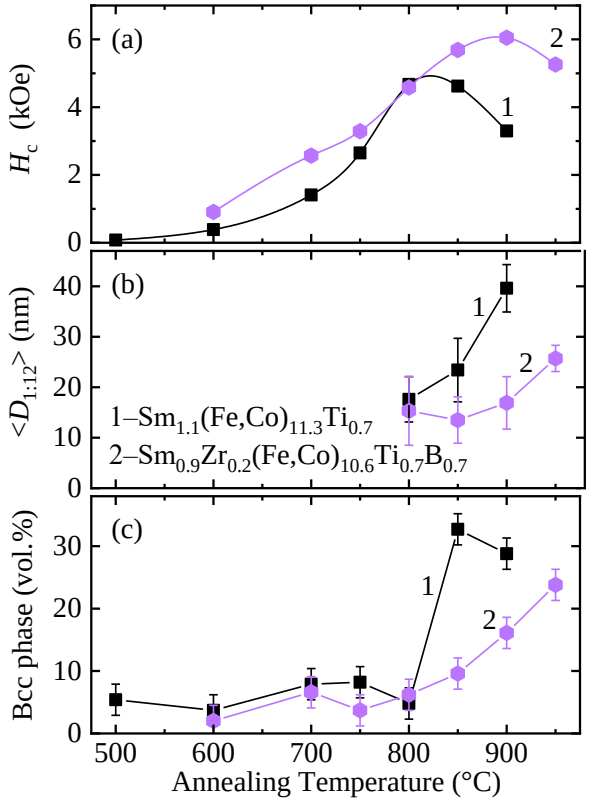

Fig. 8. Effect of 15-min annealing of $Sm_{1.1}(Fe_{0.8}Co_{0.2})_{11.3}Ti_{0.7}$ and $Sm_{0.9}Zr_{0.2}(Fe_{0.8}Co_{0.2})_{10.6}Ti_{0.7}B_{0.7}$ ribbons on (a) coercivity, (b) Scherrer average size of 1:12 crystallites and (c) fraction of magnetically soft bcc phase.

SEM micrographs in Fig. 9 compare fractured surfaces of the same two melt-spun alloys annealed at 900 °C. The comparison confirms that the modification with (B,Zr) inhibits growth of the 1:12 crystallites. It must be noted, however, that the average crystallite sizes estimated based on the SEM data, 83 nm for the parent alloy and 45 nm for the modified alloy, are significantly larger than, respectively, 39.6(4.7) nm and 16.9(5.2) nm obtained from the XRD peak broadening. This mismatch may be due to both the missing the smallest crystallites in the fractured sample and the chemical inhomogeneity of the $Sm(Fe,Ti)_{12}$-based compound, which is known to exist in a range of compositions [7,10]. If the 15-min annealing of a melt-spun alloy had not ensured the perfect chemical homogeneity, the 1:12 crystallites would be characterized by a range of lattice parameters leading to additional broadening of the XRD reflections. All other conditions being equal, a greater chemical inhomogeneity should be expected for a larger number of alloying elements. This may be the reason why the discrepancy between the Scherrer crystallite size and the crystallite size estimated based on the SEM data is greater for the $Sm_{0.9}Zr_{0.2}(Fe,Co)_{10.6}Ti_{0.7}B_{0.7}$ alloy than for the $Sm_{1.1}(Fe,Co)_{11.3}Ti_{0.7}$ alloy.

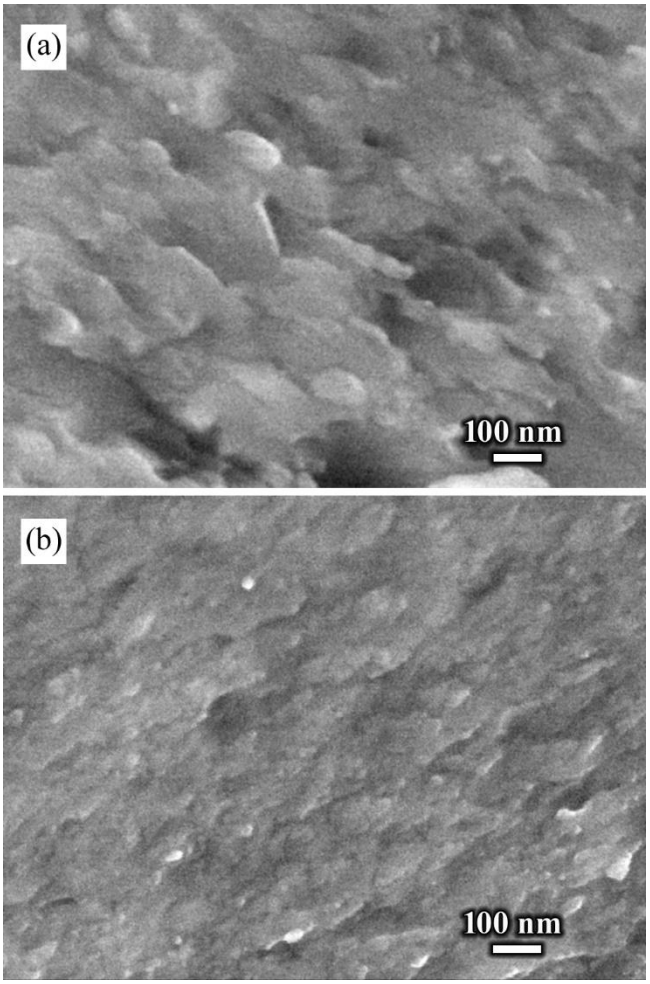

Fig. 9. Fractures of (a) $Sm_{1.1}(Fe_{0.8}Co_{0.2})_{11.3}Ti_{0.7}$ and (b) $Sm_{0.9}Zr_{0.2}(Fe_{0.8}Co_{0.2})_{10.6}Ti_{0.7}B_{0.7}$ melt-spun ribbons annealed at 900 °C for 15 min.

3.3. Effect of annealing time

The continuous evolution of the principal 1:7 and 1:12 phases in the melt-spun alloys subjected to heat treatment was demonstrated in subsection 3.1 by varying the annealing temperature. However, at any particular temperature, the metastable structures of the as-spun alloys must evolve towards the corresponding temperature-specific phase equilibrium. This means that even above the temperature of the 1:7 → 1:12 transformation it is not certain that the alloy evolution will follow the same pathway when annealed for a long time isothermally. Figure 10 presents demagnetization curves of the $Sm_{0.9}Zr_{0.2}(Fe,Co)_{10.6}Ti_{0.7}B_{0.7}$ ribbons annealed at 800 °C for increasing time intervals, up to 60 min. The increase of the H_c and decrease of the B_r with the annealing time are qualitatively similar to the changes observed in the same alloy with increasing the T_a [see Fig. 6(b)]. To compare the isochronal and isothermal treatments quantitatively, the lattice parameters of the 1:12 structure determined by analyzing the XRD data are plotted in the same Fig. 10 against the H_c values. The resulting reasonably good match

between the data for the 15 min isochronal annealing and the data for the 800 °C isothermal annealing indicates that the two treatments are indeed equivalent.

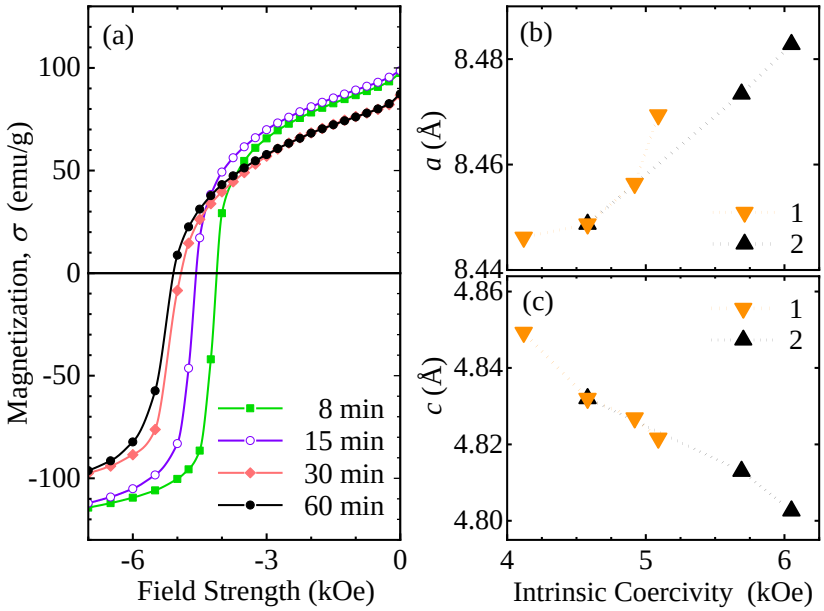

Fig. 10. (a) Room-temperature demagnetization curves of $Sm_{0.9}Zr_{0.2}(Fe_{0.8}Co_{0.2})_{10.6}Ti_{0.7}B_{0.7}$ ribbons annealed at 800 °C for the indicated time and (b,c) correlation between lattice parameters of the 1:12 phase and coercivity for ribbons of this composition: 1 – annealed for 8, 15, 30 and 60 min at 800 °C; 2 – annealed for 15 min at 800, 850 and 900 °C. All lines are guides to the eye.

3.4. Isotropic magnets produced from melt-spun ribbons

Selected ribbons were subjected to hot compaction in vacuum at the highest temperature and pressure supported by the equipment used in this study. The resulting bulk samples were sufficiently strong to withstand cutting and polishing, but their density was found to be only 6.60–6.90 g/cm^3 or 84–89% of the corresponding *ingot densities*. In agreement with the results for annealed loose ribbons, the bulk samples compacted at 650 °C had the principal phase of the 1:7 structure [Fig. S1(a), Supplementary data] and exhibited a H_c of 1–2 kOe. In order to develop the 1:12 structure as well as to increase the density, the compacted samples were subjected to an additional annealing treatment at 750–900 °C. The XRD characterization [Fig. S1(b), Supplementary data] confirmed that the 1:12 structure was indeed obtained, with only a few volume percent of the undesirable bcc phase present. Moreover, the 60 min annealing at 800–900 °C increased the density of bulk samples to 7.05–7.20 g/cm^3 or 90–93% of the ingot density. Figure 11 presents room-temperature demagnetization curves of the $Sm_{1.1}(Fe,Co)_{11.3}Ti_{0.7}$ bulk samples for all annealing conditions and Zr- and B-modified bulk samples for selected annealing conditions (see also Figs. S2–S4, Supplementary data). It is remarkable that even after annealing

at 900 °C, none of the demagnetization curves features zero-field steps, despite the relatively long annealing time of 60 min. This conclusively demonstrates that neither evaporation of Sm nor its oxidation effectively restricts annealing of *bulk* $Sm(Fe,Co,Ti)_{12}$ magnets characterized by a small surface-to-volume ratio [39] (although a thin surface layer of the annealed magnets may still need to be polished off – as it was polished off in this study).

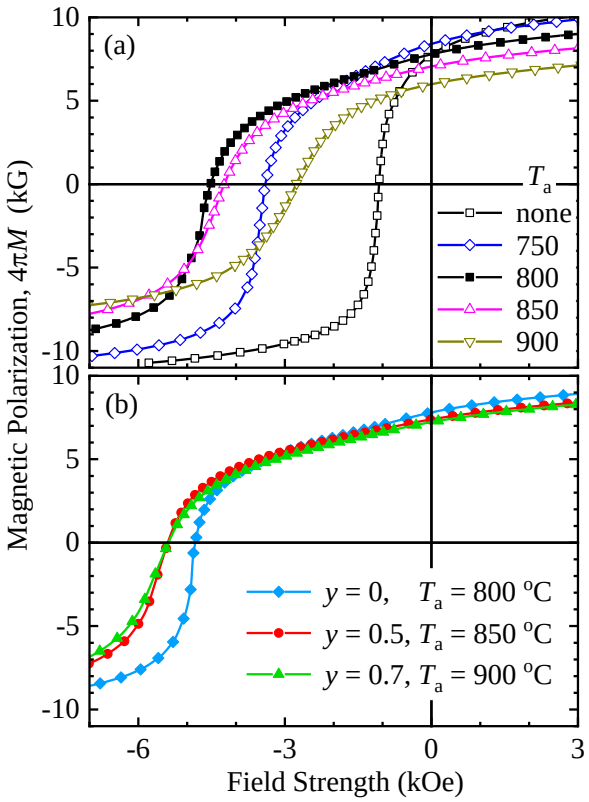

Fig. 11. Room-temperature demagnetization curves of (a) $Sm_{1.1}(Fe_{0.8}Co_{0.2})_{11.3}Ti_{0.7}$ hot-compacted bulk samples annealed at the indicated temperatures (in °C) and (b) $Sm_{0.9}Zr_{0.2}(Fe_{0.8}Co_{0.2})_{11.3-y}Ti_{0.7}B_y$ hot-compacted bulk samples for selected annealing temperatures. Annealing time in all cases was 60 min.

Evolution of the hard magnetic properties with temperature of the post-compaction annealing is shown in Fig. 12. As it was the case of the loose ribbons, H_c of the compacted ribbons prepared *without boron* begins to decline when the T_a exceeds 800 °C. On the other hand, H_c of the compacted ribbons *containing simultaneously Zr and B* continues to increase for T_a > 800 °C – reaching eventually markedly higher values. Thus, despite the fact that the B_r invariably declines with the T_a, the annealing at 850–900 °C ensured better combinations of the $(BH)_{max}$ and H_c in the compositionally modified alloys. Properties of optimally annealed bulk samples of the four different compositions are summarized in Table 1. Zirconium decreases the T_C of the magnets, whereas boron increases it – in agreement with the earlier findings [26] for

the $Sm(Fe,V,B)_{12}$ compounds. Correspondingly, measurements at elevated temperatures, summarized in Fig. 13 (the demagnetization curves are shown in Figs. S5–S8, Supplementary data) reveal that the hard magnetic properties of the Zr-modified $Sm_{0.9}Zr_{0.2}(Fe_{0.8}Co_{0.2})_{11.3}Ti_{0.7}$ magnet – characterized by the highest room-temperature $(BH)_{max}$ – decline with the temperature *most rapidly*. Conversely, simultaneous modification with Zr and B improves temperature stability of the properties. Particularly remarkable is a small value of the temperature coefficient $\beta_{175} = [H_c(175\ °C) - H_c(27\ °C)] \times 100\% / [H_c(27\ °C) \times 148\ °C]$ determined for the $Sm_{0.9}Zr_{0.2}(Fe,Co)_{10.8}Ti_{0.7}B_{0.5}$ magnet; it is equal to -0.25%/°C compared to -0.32%/°C of the Zr- and B-free magnet. At 175 °C, this isotropic $Sm_{0.9}Zr_{0.2}(Fe,Co)_{10.8}Ti_{0.7}B_{0.5}$ magnet has a H_c of 3.4 kOe and a $(BH)_{max}$ of 5.8 MGOe. If the density of this magnet is increased to 100% or 7.77 g/cm^3 (for example, by compacting the ribbons at 850 °C rather than compacting them at 650 °C and then annealing at 850 °C), the $(BH)_{max}$ would be increased to 10 MGOe at room temperature and to 6.8 MGOe at 175 °C. The feasibility of the former value has been already demonstrated by Qian at al. [39], whereas the latter value is comparable to the melt-spun Nd–Fe–B alloy (7.6 MGOe at 173 °C [50]) which has almost twice the rare-earth content.

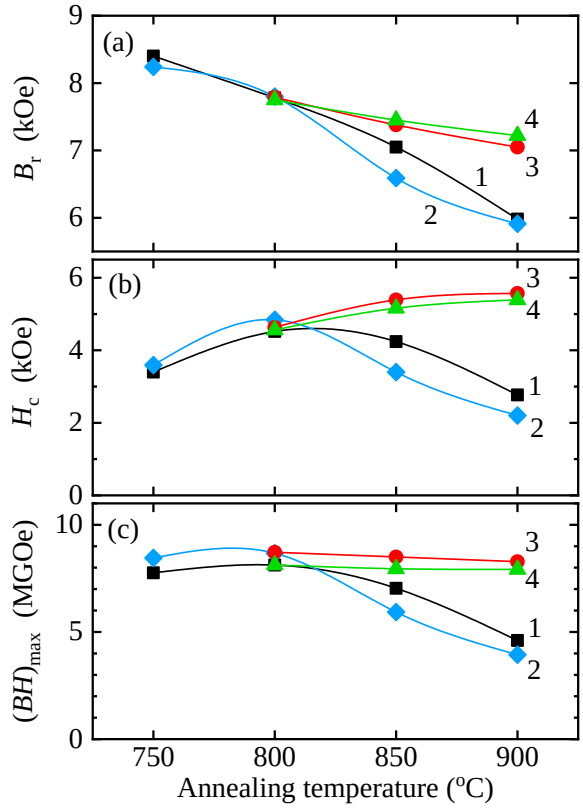

Fig. 12. Effect of 60-min annealing on (a) remanence, (b) intrinsic coercivity and (c) maximum energy product of hot-compacted bulk samples: 1 – $Sm_{1.1}(Fe_{0.8}Co_{0.2})_{11.3}Ti_{0.7}$, 2 – $Sm_{0.9}Zr_{0.2}(Fe_{0.8}Co_{0.2})_{11.3}Ti_{0.7}$, 3 – $Sm_{0.9}Zr_{0.2}(Fe_{0.8}Co_{0.2})_{10.8}Ti_{0.7}B_{0.5}$, 4 – $Sm_{0.9}Zr_{0.2}(Fe_{0.8}Co_{0.2})_{10.6}Ti_{0.7}B_{0.7}$.

Table 1. Density values ρ and magnetic properties of selected $(Sm_{1-x}Zr_x)_{1.1}(Fe_{0.8}Co_{0.2})_{11.3-y}Ti_{0.7}B_y$ magnets compacted from melt-spun ribbons. Annealing at temperature T_a was performed for 60 min; β_{175} is the temperature coefficient of H_c between 27 and 175 °C.

x	y	T_a (°C)	ρ (g/cm^3)	T_C (°C)	B_r (kG)	H_c (kOe)	$(BH)_{max}$ (MGOe)	β_{175} (%/°C)
0	0	800	7.13	518(2)	7.8	4.5	8.1	-0.32
0.2	0	800	7.05	508(1)	7.8	4.8	8.7	-0.33
0.2	0.5	850	7.15	525(2)	7.4	5.4	8.5	-0.25
0.2	0.7	900	7.19	535(2)	7.2	5.4	7.9	-0.30

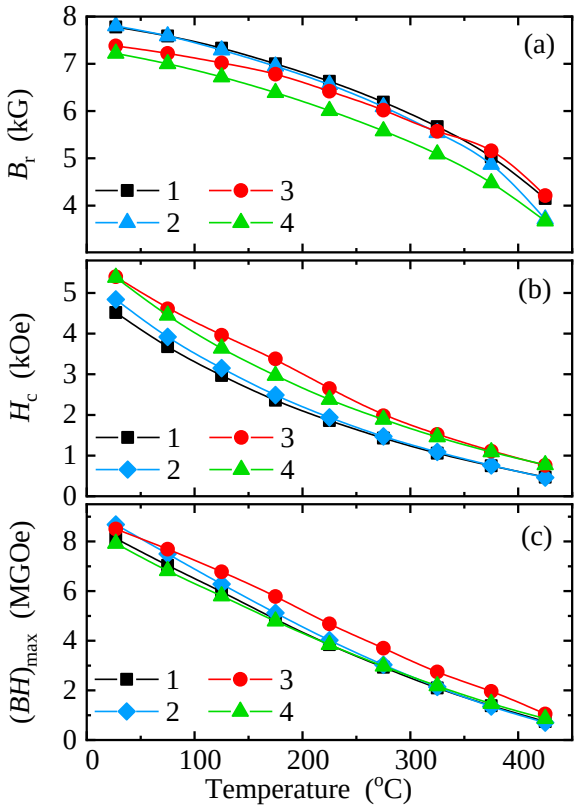

Fig. 13. Temperature dependence of (a) remanence, (b) intrinsic coercivity and (c) maximum energy product measured for bulk samples hot-compacted and subsequently annealed at T_a for 60 min: 1 – $Sm_{1.1}(Fe_{0.8}Co_{0.2})_{11.3}Ti_{0.7}$, T_a= 800 °C; 2 – $Sm_{0.9}Zr_{0.2}(Fe_{0.8}Co_{0.2})_{11.3}Ti_{0.7}$, T_a= 800 °C; 3 – $Sm_{0.9}Zr_{0.2}(Fe_{0.8}Co_{0.2})_{10.8}Ti_{0.7}B_{0.5}$, T_a= 850 °C; 4 – $Sm_{0.9}Zr_{0.2}(Fe_{0.8}Co_{0.2})_{10.6}Ti_{0.7}B_{0.7}$, T_a= 900 °C.

4. Conclusion

Modifications with boron and zirconium did not dramatically increase coercivity of the $Sm(Fe,Co)_{11.3}Ti_{0.7}$ alloy, and there are no indications that the improvement associated with boron-rich grain-boundary phases in epitaxially grown thin films [31] can be reproduced in melt-spun ribbons. Modification of the ribbons with both elements did, however, lead to a moderate

increase in the coercivity, supposedly by allowing for a more complete formation of the 1:12 compound without excessive coarsening of the microstructure. This, in turn, allowed for manufacturing of isotropic magnets exhibiting a low temperature coefficient of coercivity and actually storing more magnetic energy than any reported anisotropic 1:12 magnet. Despite this modest progress, the task of utilizing the potential of the $Sm(Fe,Co,Ti)_{12}$ compounds remains outstanding.

Acknowledgement

This work was supported by the U.S. Department of Energy [grant number DE-FG02-90ER45413].

References

[1] T. Kuno, S. Suzuki, K. Urushibata, K. Kobayashi, N. Sakuma, M. Yano, A. Kato, A. Manabe, $(Sm,Zr)(Fe,Co)_{11.0\text{-}11.5}Ti_{1.0\text{-}0.5}$ compounds as new permanent magnet materials. AIP Adv. 6 (2016) 025221. http://doi.org/10.1063/1.4943051.

[2] Y. Hirayama, Y.K. Takahashi, S. Hirosawa, K. Hono, Intrinsic hard magnetic properties of $Sm(Fe_{1\text{-}x}Co_x)_{12}$ compound with the $ThMn_{12}$ structure, Scr. Mater. 138 (2017) 62–65. http://doi.org/10.1016/j.scriptamat.2017.05.029.

[3] P. Tozman, H. Sepehri-Amin, Y.K. Takahashi, S. Hirosawa, K. Hono, Intrinsic magnetic properties of $Sm(Fe_{1\text{-}x}Co_x)_{11}Ti$ and Zr-substituted $Sm_{1\text{-}y}Zr_y(Fe_{0.8}Co_{0.2})_{11.5}Ti_{0.5}$ compounds with $ThMn_{12}$ structure toward the development of permanent magnets, Acta Mater. 153 (2018) 354–363. https://doi.org/10.1016/j.actamat.2018.05.008.

[4] P. Tozman, Y.K. Takahashi, H. Sepehri-Amin, D. Ogawa, S. Hirosawa, K. Hono, The effect of Zr substitution on saturation magnetization in $(Sm_{1\text{-}x}Zr_x)(Fe_{0.8}Co_{0.2})_{12}$ compound with the $ThMn_{12}$ structure, Acta Mater., 178 (2019) 114–121. https://doi.org/10.1016/j.actamat.2019.08.003.

[5] M. Hagiwara, N. Sanada, S. Sakurada, Structural and magnetic properties of rapidly quenched $(Sm,R)(Fe,Co)_{11.4}Ti_{0.6}$ (R = Y, Zr) with $ThMn_{12}$ structure, AIP Adv. 9 (2019) 035036. https://doi.org/10.1063/1.5079949.

[6] S. Sugimoto, A. Kojima, M. Okada, M. Homma, Enhancement of magnetic properties of Sm(Fe,Co,Ti)12 melt-spun ribbons by refining crystallized grains, Mater. Trans. 32 (1991) 1180–1183. https://doi.org/10.2320/matertrans1989.32.1180.

[7] B. Reinsch, B. Grieb, E.-Th. Henig, G. Petzow, Phase relations in the system Sm – Fe – Ti and the consequences for the production of permanent magnets, IEEE Trans. Magn. 28 (1992) 2832–2834. https://doi.org/10.1109/20.179642.

[8] K. Kobayashi, S. Suzuki, T. Kuno, K. Urushibata, N. Sakuma, M. Yano, T. Shouji, A. Kato, A. Manabe, The stability of newly developed $(R,Zr)(Fe,Co)_{12\text{-}x}Ti_x$ alloys for permanent magnets, J. Alloys Compd. 694 (2017) 914–920. http://doi.org/10.1016/j.jallcom.2016.09.311.

[9] Y. Harashima, T. Fukazawa, H. Kino, T. Miyake, Effect of R-site substitution and the pressure on stability of RFe_{12}: A first-principles study, J. Appl. Phys. 124 (2018) 163902. https://doi.org/10.1063/1.5050057.

[10] A. C. Neiva, F. P. Missell, B. Grieb, E.-Th. Henig and G. Petzow, Phase equilibria around $SmFe_{11}Ti$ at 1000 °C, J. Less-Common Met. 170 (1991) 293–299. https://doi.org/10.1016/0022-5088(91)90331-W.

[11] F. Maccari, L. Schäfer, I. Radulov, L.V.B. Diop, S. Ener, E. Bruder, K. Skokov, O. Gutfleisch, Rapid solidification of $Nd_{1+X}Fe_{11}Ti$ compounds: Phase formation and magnetic properties, Acta Mater., 180 (2019) 15–23. https://doi.org/10.1016/j.actamat.2019.08.057.

[12] D. Palanisamy, S. Ener, F. Maccari, L. Schäfer, K.P. Skokov, O. Gutfleisch, D. Raabe, B. Gault, Grain boundary segregation, phase formation, and their influence on the coercivity of rapidly solidified $SmFe_{11}Ti$ hard magnetic alloys, Phys. Rev. Mater. 4 (2020) 054404. https://doi.org/10.1103/PhysRevMaterials.4.054404.

[13] H. Sun, Y. Otani, J.M.D. Coey, C.D. Meekison, J.P. Jakubovics, Coercivity and microstructure of melt-spun $Sm(Fe_{11}Ti)$, J. Appl. Phys., 67 (1990) 4659–4661. https://doi.org/10.1063/1.344845.

[14] Y.Z. Wang, G.C. Hadjipanayis, Magnetic properties of Sm–Fe–Ti–V alloys, J. Magn. Magn. Mater. 87 (1990) 375–378. https://doi.org/10.1016/0304-8853(90)90774-K.

[15] J. Wecker, M. Katter, K. Schnitzke, L. Schultz, Magnetic hardening of Sm-Fe-Ti alloys, J. Appl. Phys. 67 (1990) 4951–4953. https://doi.org/10.1063/1.344744.

[16] J. Ding, M. Rosenberg, Crystallized melt spun $Sm(Fe_{10-x}Co_x)_{11}Ti$ alloys with $(BH)_{max}$ products larger than 90 kJm-3 (11.3 MGOe), J. Less-Common Metals 161 (1990) 263–268. https://doi.org/10.1016/0022-5088(90)90036-J.

[17] Q.F. Xiao, X.K. Sun, D.Y. Geng, L. Wei, Z.D. Zhang, Y.C. Chuang, Structure and magnetic properties of rapidly quenched Sm–Fe–Ti alloys, J. Magn. Magn. Mater. 140–144 (1995) 1093-1094. https://doi.org/10.1016/0304-8853(94)01251-2.

[18] I. Ryzhikhin, S. Andreev, M. Semkin, N. Selezneva, A. Volegov, N. Kudrevatykh, Structure and magnetic properties of $(Sm_{1-x}Zr_x)Fe_{11}Ti$ (x = 0–0.2) alloys, J. Phys.: Conf. Ser. 1389 (2019) 012117. https://doi.org/10.1088/1742-6596/1389/1/012117.

[19] D.S. Neznakhin, S.V. Andreev, M.A. Semkin, N.V. Selezneva, M.N. Volochaev, A.S. Bolyachkin, N.V. Kudrevatykh, A.S. Volegov, Structure and magnetic properties of $(Sm_{0.9}Zr_{0.1})Fe_{11}Ti$ alloys with $ThMn_{12}$-type structure, J. Magn. Magn. Mater. 484 (2019) 212–217. https://doi.org/10.1016/j.jmmm.2019.04.030.

[20] A.G. Popov, A.V. Protasov, V.S. Gaviko, D.A. Kolodkin, P.B. Terentev, E.G. Gerasimov, T. Zhang, C. Jiang, Magnetic properties of melt-spun ribbons $(Sm_{1-x}Zr_x)(Fe_{0.92}Ti_{0.08})_{10}$ with $ThMn_{12}$ structure and their hydrides, J. Rare Earths 37 (2019) 1066–1071. https://doi.org/10.1016/j.jre.2019.04.007

[21] L. Zhao, C. Li, X. Zhang, S. Bandaru, K. Su, X. Liu, Q. Zhou, L. Li, J.M. Greneche, J. Jin, M. Yan, Effects of Sm content on the phase structure, microstructure and magnetic properties

of the $Sm_xZr_{0.2}(Fe_{0.8}Co_{0.2})_{11.5}Ti_{0.5}$ (x = 0.8–1.4) alloys, J. Alloys Comp. 828 (2020) 154428. https://doi.org/10.1016/j.jallcom.2020.154428.

[22] T. Kuno, T. Yamamoto, K. Urushibata, K. Kobayashi, S. Sugimoto, Preparation of high-coercivity magnetic powder via heat treatment of a rapidly quenched amorphous starting compound with a $ThMn_{12}$ structure, Mater. Trans. 61 (2020) 657–662. https://doi.org/10.2320/matertrans.MT-M2019356.

[23] E.W. Singleton, J. Strzeszewski, G.C. Hadjipanayis, High coercivity in rapidly quenched $Sm(Fe,T)_{12}$-type magnets, Appl. Phys. Lett. 54 (1989) 1934–1936. https://doi.org/10.1063/1.101501.

[24] M.S. Anagnostou, D. Niarchos, Large coercivities in melt-spun Sm–Fe–Ti type magnets, J. Magn. Magn. Mater. 88 (1990) 100–104. https://doi.org/10.1016/S0304-8853(97)90018-4.

[25] D. Zhang, Z.D. Zhang, Y.C. Chuang, B.S. Zhang, J.L. Yang, H.L. Du, Neutron diffraction study of the boride $Y(Fe_{11.04}Ti_{0.52}B_{0.43})Ti_{0.39}$: a new phase of a $ThMn_{12}$-type intermetallic interstitial compound, J. Phys.: Condens. Matter 7 (1995) 2587–2592. https://doi.org/10.1088/0953-8984/7/13/008.

[26] Y.C. Chuang, D. Zhang, T. Zhao, Z.D. Zhang, W. Liu, X.G. Zhao, X.K. Sun, F.R. de Boer, Structure and magnetic properties of $R(FeVB)_{12}$ compounds, J. Alloys Compd. 221 (1995) 60–64. https://doi.org/10.1016/0925-8388(94)01430-2.

[27] D. Odkhuu, T. Ochirkhuyag, S.C. Hong, Enhancing energy product and thermal stability of $SmFe_{12}$ by interstitial doping, Phys. Rev. Appl. 13 (2020) 054076. http://dx.doi.org/10.1103/PhysRevApplied.13.054076.

[28] Y. Horiuchi, S. Sakurada, Structural and magnetic properties of rapidly quenched $(Sm,Zr)(Fe,Co)_{11}B_x$ (x = 0–1) ribbons, J. Appl. Phys. 109 (2011) 07A733. http://doi.org/10.1063/1.3562914.

[29] C. Zheng, D. Yu, K. Li, Y. Luo, J. Jin, S. Lu, H. Li, Y. Mao, N. Quan, Effect of boron additions on phase formation and magnetic properties of $TbCu_7$-type melt spun SmFe ribbons, J. Magn. Magn. Mater. 412 (2016) 89–94. http://doi.org/10.1016/j.jmmm.2016.03.082.

[30] M. Katter, J. Wecker, L. Schultz, Structural and hard magnetic properties of rapidly solidified Sm–Fe–N, J. Appl. Phys. 70 (1991) 3188–3196. https://doi.org/10.1063/1.349302.

[31] H. Sepehri-Amin, Y. Tamazawa, M. Kambayashi, G. Saito, Y.K. Takahashi, D. Ogawa, T. Ohkubo, S. Hirosawa, M. Doi, T. Shima, K. Hono, Achievement of high coercivity in $Sm(Fe_{0.8}Co_{0.2})_{12}$ anisotropic magnetic thin film by boron doping, Acta Mater. 194 (2020) 337–342. https://doi.org/10.1016/j.actamat.2020.05.026.

[32] Y. Wang, G.C. Hadjipanayis, A. Kim, N.C. Liu, D.J. Sellmyer, Magnetic and structural studies in Sm-Fe-Ti magnets, J. Appl. Phys. 67 (1990) 4954–4956. https://doi.org/10.1063/1.344745.

[33] I. Dirba, J. Li, H. Sepehri-Amin, T. Ohkubo, T. Schrefl, K. Hono, Anisotropic, single-crystalline $SmFe_{12}$-based microparticles with high roundness fabricated by jet-milling, J. Alloys Compd. 804 (2019) 155–162. https://doi.org/10.1016/j.jallcom.2019.06.365.

[34] A.M. Schönhöbel, R. Madugundo, A.M. Gabay, J.M. Barandiarán, G.C. Hadjipanayis, The Sm-Fe-V based 1:12 bulk magnets, J. Alloys Compd. 791 (2019) 1122–1127. https://doi.org/10.1016/j.jallcom.2019.03.249.

[35] D. Simon, H. Wuest, S. Hinderberger, T. Koehler, A. Marusczyk, S. Sawatzki, L.V.B. Diop, K. Skokov, F. Maccari, A. Senyshyn, H. Ehrenberg, O. Gutfleisch, Structural and magnetic properties of $Ce_{1-x}Sm_xFe_{11-y}Ti_1V_y$, Acta Mater. 172 (2019) 131–138. https://doi.org/10.1016/j.actamat.2019.04.006.

[36] A.M. Schönhöbel, R. Madugundo, J.M. Barandiarán, G.C. Hadjipanayis, D. Palanisamy, T. Schwarz, B. Gault, D. Raabe, K. Skokov, O. Gutfleisch, J. Fischbacher, T. Schrefl, Nanocrystalline Sm-based 1:12 magnets, Acta Mater. 200 (2020) 652–658. https://doi.org/10.1016/j.actamat.2020.08.075.

[37] T. Saito, F. Watanabe, D. Nishio-Hamane, Magnetic properties of $SmFe_{12}$-based magnets produced by spark plasma sintering method, J. Alloys Comp. 773 (2019) 1018–1022. https://doi.org/10.1016/j.jallcom.2018.09.297.

[38] T. Saito, F. Watanabe, D. Nishio-Hamane, High-coercivity $Sm(Fe,V,Ti)_{12}$ bulk magnets, Mater. Res. Bull. 133 (2021) 111060. https://doi.org/10.1016/j.materresbull.2020.111060.

[39] H.D. Qian, J.T. Lim, J.W. Kim, Y. Yang, K.M. Cho, J. Park, C.J. Choi, Phase transformation and magnetic properties of fully dense $Sm(Fe_{0.8}Co_{0.2})_{11}Ti$ bulk magnets, Scr. Mater. 193 (2021) 17–21. https://doi.org/10.1016/j.scriptamat.2020.10.030.

[40] W. Kraus, G. Nolze, Powder Cell - a program for the representation and manipulation of crystal structures and calculation of the resulting X-ray powder patterns, J. Appl. Crystallogr. 29 (1996) 301–303. https://doi.org/10.1107/S0021889895014920.

[41] K. He, N. Chen, C. Wang, L. Wei, J. Chen, Method for determining crystal grain size by X-ray diffraction, Cryst. Res. Technol. 2018, 53, 1700157. https://doi.org/10.1002/crat.201700157.

[42] A. Aharoni, Demagnetizing factors for rectangular ferromagnetic prisms, J. Appl. Phys. 83 (1998) 3432–3434. https://doi.org/10.1063/1.367113.

[43] K.H.J. Buschow, A.S. van der Goot, Composition and crystal structure of hexagonal Cu-rich rare earth-copper compounds, Acta Crystallogr. B 27 (1971) 1085–1088. https://doi.org/10.1107/S0567740871003558.

[44] L. Bessais, C. Djega-Mariadassou, Structure and magnetic properties of nanocrystalline $Sm(Fe_{1-x}Co_x)_{11}Ti$ ($x \leq 2$), Phys. Rev. 63 (2001) 054412. https://doi.org/10.1103/PhysRevB.63.054412.

[45] B.P. Hu, H.S. Li, J.M.D. Coey, Relationship between $ThMn_{12}$ and Th_2Ni_{17} structure types in the $YFe_{11-x}Ti_x$ alloy series, J. Appl. Phys. 67 (1990) 4838–4840. http://doi.org/10.1063/1.344753.

[46] H. Saito, M. Takahashi, T. Wakiyama, Magnetic properties and structure change from tetragonal to hexagonal for the rapidly quenched $SmTiFe_{11}$ alloy ribbons, J. Appl. Phys. 64 (1988) 5965–5967. http://doi.org/10.1063/1.342164.

[47] H. Suzuki, Structural analysis and magnetic properties of lattice distortions from hexagonal to tetragonal systems in non-equilibrium Y–Fe alloys, Intermetallics 119 (2020) 106713. https://doi.org/10.1016/j.intermet.2020.106713.

[48] A. Urzhumtsev, M. Anikin, E. Tarasov, M. Semkin, M. Cherepkov, N. Kudrevatykh, A. Zinin, V. Moskalev, Effect of alloying elements (Zr,Hf,Co), heat and mechanical treatment conditions on the phase composition and magnetic properties of $SmFe_{11}Ti$ compounds with $ThMn_{12}$ structure, EPJ Web Conf. 185 (2018) 04026. https://doi.org/10.1051/epjconf/201818504026.

[49] M. Matzinger, j. Fidler, A. Fujita, I.R. Harris, Microstructure of solid-HDDR Nd-Fe-B:Zr magnets, J. Magn. Magn. Mater. 157/158 (1996) 54–56. https://doi.org/10.1016/0304-8853(95)01134-X.

[50] J.J. Croat, J.F. Herbst, R.W. Lee, F.E. Pinkerton, Pr-Fe and Nd-Fe-based materials: A new class of high-performance permanent magnets, J. Appl. Phys. 55 (1984) 2078–2082. https://doi.org/10.1063/1.333571.